remote sensing

MDPI

Article

The Physiological and Structural Responses of African Vegetation to Extreme Drought Revealed by Multi-Spectral Satellite Remote Sensing

Yuqiao Zhao [1,2] and Xiang Zhang [1,2,*]

[1] National Engineering Research Center of Geographic Information System, School of Geography and Information Engineering, China University of Geosciences, Wuhan 430074, China; zhaoyuqiao@cug.edu.cn
[2] Shenzhen Research Institute, China University of Geosciences, Shenzhen 518063, China
* Correspondence: zhangxiang76@cug.edu.cn; Tel.: +86-158-7147-2170

Highlights

What are the main findings?

- Vegetation drought responses are decomposed into physiological and structural anomalies, revealing fine-scale functional impacts of drought beyond traditional methods.
- Vegetation physiological components explained most of the functional responses during drought, and physiological anomalies accounted for over 88% of total vegetation anomalies during drought peaks, highlighting their dominant role in early-stage drought response.

What are the implications of the main findings?

- Physiological responses consistently outperform structural responses before, during, and after drought peaks, with intensified fluctuations at peak stress, underscoring vegetation's prioritization of rapid physiological adjustments. This study advocates for the integration of physiological remote sensing indicators to establish a more sensitive early warning system for drought.
- Spatial vulnerability patterns and quantified climate drivers directly support tailored water and climate adaptation strategies.

Abstract

African vegetation responses to extreme drought represent a key challenge for global change research and sustainable water–land resource management. Satellite remote sensing provides long-term observations of vegetation dynamics, yet conventional analyses focus on vegetation structural, greenness, or productivity changes, lacking of understanding on physiological adaptation. This study applies a multi-model framework integrating high-temporal-resolution (4-day) and multi-spectral satellite data with machine learning to disentangle structural and physiological responses across Central and Western Africa. Three key indicators were used: evapotranspiration (ET), relative solar-induced chlorophyll fluorescence (SIF_{rel}), and the ratio of midday to midnight vegetation optical depth (VOD_{ratio}), which respectively, represent water flux, photosynthetic activity, and water regulation. A random forest model, combined with SHapley Additive exPlanations (SHAP) analysis, was used to separate vegetation anomaly signals and identify key climatic controls. The results reveal pronounced differences in vegetation responses between arid and humid climatic regions. In arid regions, near-infrared reflectance of vegetation (NIRv) and solar-induced chlorophyll fluorescence (SIF) exhibited clear negative anomalies and significant pre-drought declines, accompanied by marked changes in vegetation optical

Check for updates

Academic Editors: Baodong Xu, Hu Zhang and Yelu Zeng

Received: 11 December 2025
Revised: 23 January 2026
Accepted: 27 January 2026
Published: 2 February 2026

Copyright: © 2026 by the authors. Licensee MDPI, Basel, Switzerland. This article is an open access article distributed under the terms and conditions of the Creative Commons Attribution (CC BY) license.

depth (VOD), indicating canopy structural damage and reduced photosynthetic activity. In contrast, trend analysis revealed that although SIF and NIRv in humid regions showed relatively strong responses during the pre-drought phase, they did not exhibit significant trends after the drought peak, and changes in VOD were comparatively small, suggesting that higher water availability partially buffered the prolonged impacts of drought on vegetation structure and function. Process analysis showed that three months before and after drought peaks, physiological indicators exhibited strong anomalies that closely tracked drought duration. SIF_{rel}, ET signals peaked earlier than water-content anomalies (VOD_{ratio}), suggesting a two-phase regulation strategy: early stomatal closure followed by delayed deep-root water uptake. Physiological anomalies accounted for over 88% of total vegetation anomalies during drought peaks, highlighting their dominant role in early-stage drought response. Precipitation and temperature emerged as primary drivers, explaining 76.8% of photosynthetic variation, 60.3% of ET variation, and 53.9% of water-content variation in the development. The recovery is influenced by the duration of drought and the regrowth of vegetation. By explicitly decoupling physiological and structural vegetation responses, this study provides refined, process-based insights into African ecosystem adaptation to water stress. These findings contribute to more accurate drought monitoring, water availability assessment, and climate adaptation strategies, directly supporting sustainable water and land management goals.

Keywords: drought; vegetation anomaly decomposition; random forest model; SHAP method; spatiotemporal heterogeneity; ecosystem response

1. Introduction

Drought is a natural phenomenon that occurs when available water resources are significantly below normal levels and cannot meet current water demand. It is a natural disaster characterized by long duration, high frequency, and a wide-ranging impact. As a global environmental issue, drought not only poses a severe threat to agriculture, industry, and human life but also has profound effects on the stability and functionality of ecosystems. Recent studies have shown that, with the intensification of climate change, the frequency and intensity of drought events are expected to significantly increase globally [1]. This projected increase in drought frequency and intensity is likely to have significant impacts on the composition, function, and resilience of terrestrial ecosystems, especially in high-risk drought regions such as sub-Saharan Africa and the tropical rainforest areas of Central Africa [2].

In this context, vegetation, as a core component of terrestrial ecosystems, plays a key role not only in maintaining soil and water conditions and regulating the climate, but also in controlling the energy balance and material cycles of ecosystems through processes such as photosynthesis, transpiration, and carbon fixation [3]. However, extreme drought events significantly weaken vegetation's physiological functions and growth processes, leading not only to a decline in productivity but also potentially triggering large-scale vegetation mortality, which has profound implications for regional and even global carbon cycles [4]. The response of vegetation to drought stress is a complex physiological regulation process involving various mechanisms, such as root water absorption, stomatal regulation, photosynthesis inhibition, and leaf growth limitation [5]. Therefore, in-depth research into the response mechanisms of vegetation to drought stress is not only helpful in understanding the internal interactions of terrestrial ecosystems but also crucial for assessing ecosystem health and formulating scientific ecological protection and management policies.

In order to better understand vegetation's response mechanisms under extreme climate conditions such as drought, multi-functional water-carbon coupling indices have become key tools for linking climate drivers to ecosystem responses. Through complex interactions, meteorological factors such as precipitation, temperature, and solar radiation significantly affect vegetation's physiological activities [6]. For example, precipitation directly affects the growth dynamics of vegetation in drought-prone areas, temperature regulates physiological processes by influencing plant photosynthesis and respiration, and solar radiation provides the energy source for photosynthesis, thus affecting its carbon assimilation capacity [7]. During drought, vegetation's functional responses mainly manifest in three forms: (1) regulation of photosynthesis, reflecting how plants cope with water stress by adjusting stomatal opening and closing, as well as chlorophyll content; (2) changes in transpiration, where plants adjust stomatal conductance to reduce water loss, maintaining water balance in water-scarce environments [8]; and (3) water regulation, where vegetation regulates internal water distribution through processes such as root water absorption and leaf transpiration to ensure normal physiological function. These functional responses are interwoven, forming a comprehensive adaptive mechanism for vegetation during drought. At the same time, vegetation's structural characteristics, such as the LAI, and their responses to these environmental factors and feedback regulation are also key areas of research [9]. The LAI, as an important indicator of vegetation's photosynthetic potential, often shows a significant decrease during drought, affecting vegetation's ability to absorb solar radiation [10]. Therefore, understanding vegetation's structural responses, especially the interactions between multiple functional processes such as photosynthesis, transpiration, and water regulation, is crucial for revealing the impacts of drought on ecosystems.

In order to more comprehensively study vegetation's responses under extreme climate conditions such as drought, especially the interactions between multiple functional processes like photosynthesis, transpiration, and water regulation, the rapid development of remote sensing technology has provided new research tools. These technologies can efficiently acquire structural and physiological information of vegetation in a short amount of time and enable quantitative climate change response assessments [11,12]. Previous studies have demonstrated that remotely sensed indicators can capture different aspects of vegetation drought responses. For example, Xu et al. observed that SIF sensitivity to drought varies along a drought gradient, with the highest correlation in semi-arid ecosystems [13]. Hoek et al. further revealed contrasting drought response strategies between forests and grasslands, highlighting the complexity of vegetation responses across ecosystems [14].

Despite these advances, current understanding of vegetation responses to drought remains incomplete, particularly with respect to the coordinated changes among multiple ecosystem functions. A comparative synthesis of previous studies on vegetation drought responses, including differences in indicators, spatial–temporal scales, and the limited disentanglement of physiological and structural responses, is provided in Table A1 (Appendix A). A major challenge is that remotely sensed signals often reflect a combination of physiological regulation and structural adjustment processes, making it difficult to disentangle their respective contributions during drought events. These issues hinder a comprehensive and mechanistic understanding of drought impacts on vegetation. Vegetation's physiological responses (such as stomatal closure and photosynthesis inhibition) typically occur before structural changes (such as leaf area reduction) and are more sensitive during the early stages of drought [5]. The timeliness and independence of these physiological responses make them an important indicator for predicting the impact of drought on vegetation [15]. However, current remote sensing signal is driven simultaneously by physiological and structural responses of vegetation, leading to misunderstandings of drought responses. For example, the VOD signal is driven by both structural and physiological factors. Structural

changes are mainly reflected in changes in leaf area and canopy density, while physiological responses are manifested through changes in plant water regulation and photosynthetic efficiency [16–18]. Therefore, by separating physiological and structural responses, we can more accurately assess the dynamic changes in vegetation under drought stress and gain a deeper understanding of changes in ecosystem function.

To achieve this goal, this study uses a random forest method based on multiple remote sensing data to isolate physiological and structural responses. In particular, multi-source remote sensing datasets with high temporal resolution (every 4 days) and spatial precision (0.05°), using a random forest model to analyze the physiological response network of vegetation in Central and West Africa under drought stress between 2012 and 2020. The study focuses on revealing: (1) the multi-process synergy pattern of photosynthesis-transpiration-water regulation; (2) the driving mechanisms behind vegetation's physiological responses. The results will provide new methodological perspectives for assessing tropical ecosystem resilience and offer important scientific basis for future climate change adaptation strategies.

2. Materials and Methods

2.1. Study Area

Central and Western Africa encompass a broad range of climatic zones, spanning from the humid equatorial forests of the Congo Basin to the semi-arid savannas and Sahelian grasslands in the north (Figure 1a) [19]. The region is influenced by complex atmospheric circulation systems, including the West African Monsoon and the Intertropical Convergence Zone, which govern the spatial and seasonal distribution of precipitation (Figure 1c) [19,20]. Rainfall patterns exhibit pronounced seasonality, with a single rainy season in the north and bimodal rainy seasons in the equatorial belt [21]. The Congo Basin, located in Central Africa, contains the second-largest tropical rainforest in the world, serving as a critical reservoir of carbon and biodiversity [22,23]. In contrast, the western and northern portions of the study area transition to dry savanna and Sahelian ecosystems, where vegetation productivity is tightly coupled to seasonal rainfall variability [24,25]. This north–south gradient in water availability creates diverse vegetation structures and functional strategies for coping with climate extremes (Figure 1a,d) [26].

Droughts in this region can be triggered by both ocean–atmosphere interactions, such as El Niño–Southern Oscillation events, and long-term warming trends that intensify evapotranspiration and moisture deficits (Figure 1b) [19]. Previous studies have documented severe drought episodes leading to widespread vegetation stress, reduced agricultural yields, and impacts on regional hydrological cycles [27,28]. These events often propagate through both physiological pathways—such as reductions in stomatal conductance and photosynthetic efficiency—and structural changes including canopy loss and leaf senescence [26].

Given the ecological importance and climate sensitivity of this region, Central and Western Africa provide an ideal setting to investigate the decoupled physiological and structural responses of vegetation to extreme drought. The diversity in vegetation types, water availability regimes, and climatic drivers allows for a robust assessment of drought adaptation strategies across contrasting environmental conditions.

2.2. Data Sources and Preprocessing

2.2.1. Hydrometeorological Variables

Hydrometeorological variables included precipitation, 2 m air temperature (T2M), 2 m dew point temperature, root-zone soil moisture, and evapotranspiration, all obtained from the fifth-generation European Centre for Medium-Range Weather Forecasts reanalysis dataset, ERA5-Land [29]. ERA5-Land provides high-quality global reanalysis data at

0.1° × 0.1° spatial resolution and hourly temporal resolution, enabling precise characterization of regional meteorological variability. For this study, the ERA5-Land data were aggregated to a daily scale using Google Earth Engine (GEE) to ensure processing efficiency and consistency across variables. From these meteorological inputs, we further derived two drought-related metrics: Vapor Pressure Deficit (VPD) and the Standardized Soil Moisture Index (SSMI). VPD represents the atmospheric evaporative demand and is a key driver of plant stomatal regulation and transpiration response. SSMI characterizes the hydrometeorological balance between available water and energy, providing an effective indicator of soil moisture deficit widely applied in drought monitoring.

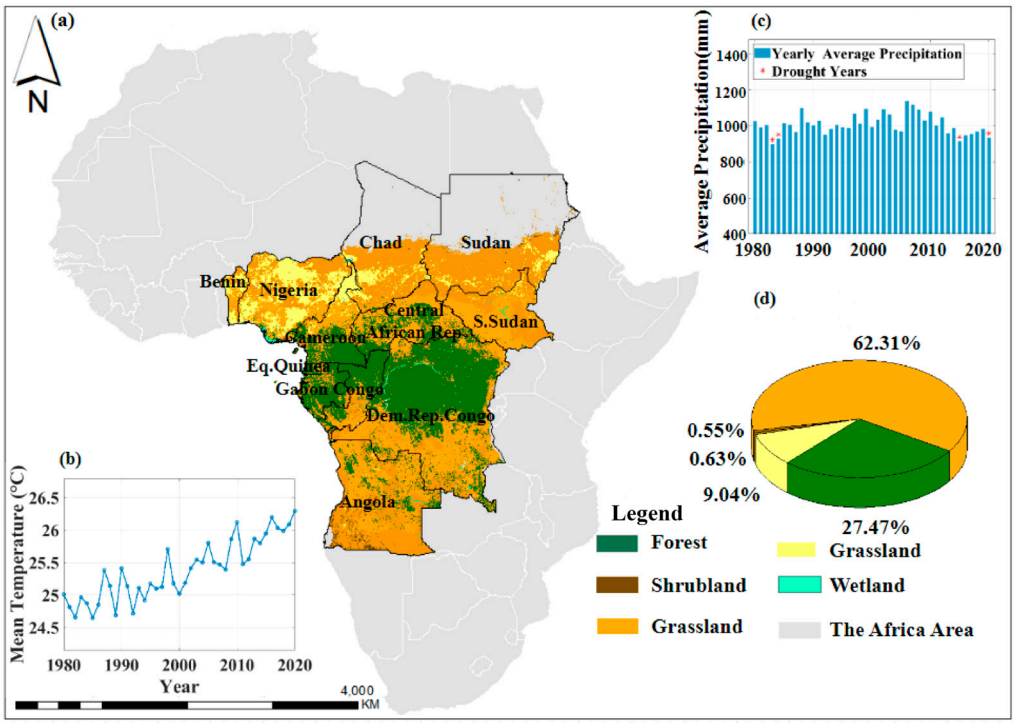


Figure 1. Overview of the study area. (**a**) The distribution of Major Vegetation Cover Classes in the study area; (**b**) Annual mean temperature; (**c**) Annual average temperature; (**d**) Poportion map of major vegetation cover classes.

2.2.2. Photosynthetic Indicators

Vegetation photosynthetic activity was characterized using SIF data from the CSIF dataset [26]. CSIF leverages a neural network approach that integrates hyperspectral observations with environmental variables to generate globally continuous SIF estimates. Two SIF products were used: SIF_{inst}—instantaneous SIF under clear-sky conditions, reflecting optimal photosynthetic performance; SIF_{daily}—daily SIF under all-sky conditions, representing integrated photosynthetic activity under varying meteorological conditions. Both products have a spatial resolution of 0.05° and a 4-day temporal resolution, enabling the detection of short-term photosynthetic fluctuations. To minimize the influence of Bidirectional Reflectance Distribution Function effects and variability in solar irradiance, SIF values were normalized by their corresponding NIRv to SIF_{rel}. This normalization enhances temporal and spatial comparability, making the data more directly interpretable in terms of physiological processes.

2.2.3. Vegetation Water Status Indicators

To assess vegetation water status, we employed VOD data from the LPDR v3 dataset [30], derived from passive microwave remote sensing observations. VOD is sen-

sitive to vegetation water content and aboveground biomass, and it responds directly to drought stress, particularly in non-tree vegetation [31]. We extracted midday VOD and midnight VOD to represent daytime and nighttime canopy water content, respectively. The VOD_{ratio}—defined as the ratio of midday to midnight VOD—was calculated to capture diurnal variations in canopy water status and hydraulic regulation under extreme climatic events.

2.2.4. Spatial Domain and Vegetation Classification

The study area was restricted to vegetated regions in Central and Western Africa, as defined by MODIS land-cover data. MODIS environmental variables were combined with Food and Agriculture Organization Corporate Statistical Database (FAOSTAT) datasets from the Food and Agriculture Organization (FAO) to classify vegetation into three categories: shrubs, trees, and grasslands [32]. Non-tree vegetation was analyzed separately to focus on functional types more vulnerable to drought stress.

2.2.5. Data Preprocessing and Anomaly Calculation

To ensure comparability across datasets, all variables were resampled to a spatial resolution of 0.05° and aggregated to a 4-day temporal resolution. The remote sensing and climate datasets used in this study, along with their original spatial and temporal resolutions, are summarized in Table 1. For ERA5-Land variables, which have an original spatial resolution of 0.1°, spatial upsampling was performed using a Nearest interpolation method implemented in Google Earth Engine. A multi-step preprocessing strategy was applied to extract short-term anomalies associated with extreme drought events: Deseasonalization—seasonal cycles were removed by subtracting the long-term mean for each time step; Detrending—long-term trends were removed using Locally Weighted Scatterplot Smoothing (LOESS), isolating anomalies attributable to sub-seasonal variability. The SSMI was used to define drought-affected areas, while aggregation of hourly meteorological variables and daily land variables to a 4-day scale facilitated the identification of sub-seasonal drought characteristics. Meanwhile, to address missing data caused by satellite retrieval limitations (e.g., cloud cover) or sensor gaps, we employed a Long Short-Term Memory (LSTM) neural network-based interpolation method. which was validated using a cross-validation scheme with 5% randomly masked observations. The method achieved high accuracy across Africa for the representative variables SIF (R^2 = 0.94, RMSE = 0.029) and NIRv (R^2 = 0.96, RMSE = 0.017), with comparable performance observed for other interpolated variables.

Table 1. Summary of Remote Sensing and Climate Data Sources with Spatial and Temporal Resolutions.

Parameter	Data Source	Spatial Resolution/Extent	Temporal Resolution/Extent
Temperature	ERA5-Land	0.1°, Global	daily
Rainfall	ERA5-Land	0.1°, Global	daily
Soil Moisture	ERA5-Land	0.1°, Global	daily
Radiation	ERA5-Land	0.1°, Global	daily
LAI	MCD15A3H	500 m, Global	4 days
NIRv	MCD43A4	500 m, Global	daily
SIF	CSIF	0.05°, Global	daily
ET	ERA5-Land	0.1°, Global	daily

2.3. Methods

This study adopts a multi-model collaborative framework to quantitatively disentangle vegetation structural and physiological responses to drought (Figure 2). The

workflow consists of three main steps: data preprocessing, anomaly decomposition, and driver attribution.

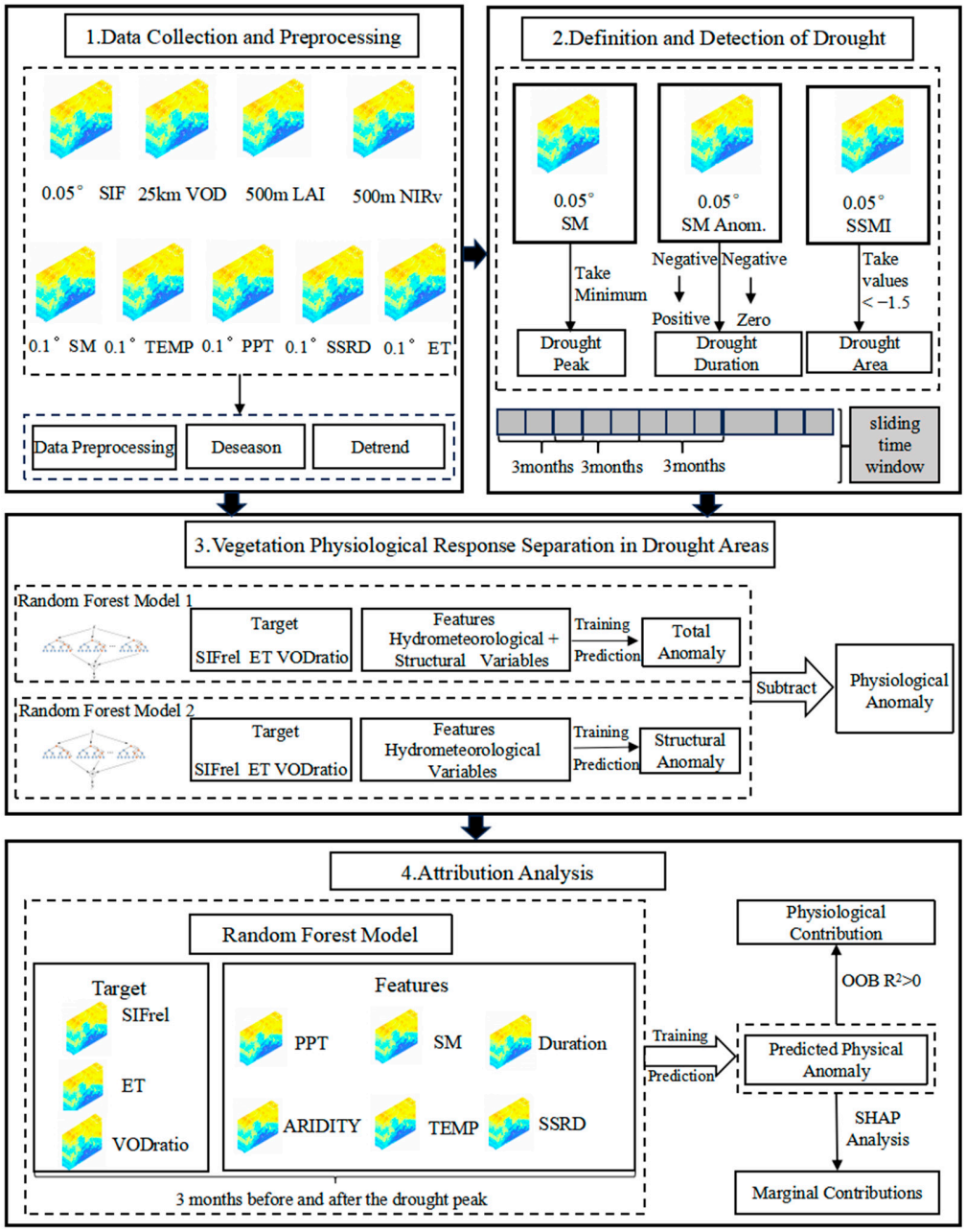


Figure 2. Quantification and Separation Framework for Vegetation Physiological and Structural Responses under Extreme Drought Stress: This framework consists of four main components: data collection and preprocessing, which involves the acquisition and organization of meteorological, soil moisture, and vegetation remote sensing data; vegetation index trajectory extraction, using a time window method to capture the variation trajectory of drought responses; vegetation physiological signal separation, focusing on distinguishing physiological signals from structural signals to enable the quantification of physiological responses; and attribution analysis, quantitatively identifying the driving factors of vegetation functional anomalies and assessing the relative contribution of each factor.

Data Preprocessing: All input variables—including SIF_{rel}, VOD_{ratio}, evapotranspiration, air temperature, precipitation, and soil moisture—were first deseasonalized and detrended to remove recurring seasonal cycles and long-term trends. This procedure

minimizes the confounding influence of external variability, ensuring that the extracted anomaly signals primarily reflect short-term drought impacts.

Anomaly Signal Decomposition: A Random Forest regression model (RF1) was trained using multi-source hydrometeorological and vegetation variables to predict the total vegetation anomaly signal. A second Random Forest model (RF2) was constructed specifically for structural attributes (e.g., LAI, NIRv) to estimate the structural anomaly signal. The physiological anomaly signal was then calculated as the residual between the total anomaly (RF1) and structural anomaly (RF2), effectively isolating the functional component from the mixed remote sensing signal.

Driver Attribution via SHAP Analysis: To identify the dominant environmental controls on physiological anomalies, we applied the SHAP method to each physiological indicator—SIF_{rel}, ET, and VOD_{ratio}. This approach quantifies the marginal contribution of each predictor (e.g., precipitation, temperature, root-zone soil moisture) and allows for phase-specific analysis across drought development and recovery periods. The SHAP results reveal both the magnitude and direction of individual drivers, as well as potential nonlinear interactions among climatic and vegetation variables.

2.3.1. Definition and Detection of Drought

To quantify drought severity, we employed the Standardized Soil Moisture Index (SSMI), which expresses soil moisture anomalies relative to their long-term climatology at each grid cell. Specifically, *SSMI* is calculated as the deviation of current soil moisture from the multi-year mean, normalized by the corresponding standard deviation:

$$SSMI_{i,j} = \frac{\theta_{i,j} - \mu\theta_i}{\sigma\theta_i} \quad (1)$$

where $SSMI_{i,j}$ is the SSMI for year j and month i, $\theta_{i,j}$ is the mean soil moisture for year j and month i, $\mu\theta_i$ is the mean of the long-term series of monthly soil moisture. σ_{θ_i} is the standard deviation of the long-time series of soil moisture at the monthly scale. For drought classification, the following thresholds were applied: mild drought ($-1.5 < SSMI \leq -1.0$), moderate drought ($-2.0 < SSMI \leq -1.5$), and severe drought ($SSMI \leq -2.0$). This classification enables spatially explicit identification of drought events and their intensity, providing a consistent framework for linking soil moisture anomalies to vegetation physiological and structural responses. In this study, drought areas were defined as grid cells with $SSMI < -1.5$.

We focused on the period from 1 January 2012 to 8 August 2020, identifying grid cells that experienced annual minimum soil moisture conditions. Drought peaks were detected based on the four lowest daily soil moisture values recorded at each grid cell during this period. Vegetation responses were analyzed during the growing season, which is defined as the period when air temperatures are above 5 °C and the mean seasonal solar-induced chlorophyll fluorescence (SIF) exceeds 0.2 mW m^{-2} sr^{-1} nm^{-1}.

Vegetation anomalies were examined using a sliding temporal window from three months before to three months after each drought peak. Drought duration was defined as the number of time steps required for soil moisture anomalies to return to zero or positive values before and after the drought peak and was used to characterize the persistence of drought and its associated vegetation responses.

2.3.2. Vegetation Anomaly Signal Decomposition

The Random Forest (RF) algorithm is a robust, non-parametric ensemble learning approach that constructs multiple high-variance decision trees through bootstrap sampling and aggregates their predictions [33]. Each regression tree is built using the Classification

and Regression Trees (CART) method, with a randomly selected subset of predictor variables considered at each split [34]. By averaging the outputs from all decision trees, RF achieves strong adaptability to nonlinear relationships and complex predictor interactions, while remaining resistant to overfitting, multicollinearity, outliers, and noise. Another key advantage is that RF requires minimal preprocessing, eliminating the need for extensive transformations or outlier removal.

In this study, RF was employed both to model physiological anomalies in SIF_{rel}, ET, and VOD_{ratio}, and to decompose the total vegetation anomaly signal into its structural and physiological components. To ensure the interpretability of model residuals and to avoid information leakage in time series data, all RF models were trained and evaluated using a time-blocked leave-out strategy rather than fitting the full time series at once. Specifically, for each grid cell, vegetation and hydrometeorological time series were divided into consecutive temporal windows. For each window, RF models were trained exclusively on data outside the target window and then applied to generate predictions only within the left-out window, yielding strictly out-of-sample estimates. This procedure was repeated across the entire time series, ensuring that all anomaly signals were derived solely from temporally independent predictions.

Within this framework, the process began by training a Random Forest model with hydrometeorological variables—such as precipitation, temperature, root-zone soil moisture, and surface solar radiation downward—as predictors, and vegetation functional indicators (SIF_{rel}, VOD_{ratio}, and ET) as responses. Based on the assumption that hydrometeorological conditions can predict vegetation physiological responses and that LAI reflects vegetation structural changes, the model predictions represent the total anomaly in vegetation.

To further isolate structural contributions, a second Random Forest model was trained using LAI as the only predictor and vegetation functional indicators (SIF_{rel}, VOD_{ratio}, and ET) as responses. Based on the assumption that LAI reflects vegetation structural changes, the model predictions represent the structural response. By subtracting the structural anomaly from the total anomaly, the physiological anomaly signal was obtained. This subtraction effectively distinguishes physiological deviations—such as changes in photosynthetic efficiency, stomatal regulation, or canopy water status—driven by climatic and hydrological variability, from structural changes caused by factors such as canopy loss or leaf senescence.

Through this decomposition, the method provides a clear separation between functional and structural vegetation responses, enabling a mechanistic understanding of drought impacts. This separation not only strengthens the theoretical foundation for drought attribution but also ensures that subsequent analyses are grounded in physiologically meaningful indicators.

2.3.3. Attribution Analysis

To uncover the driving mechanisms and spatial–temporal heterogeneity of vegetation physiological responses to drought, a Random Forest Regression model was constructed to predict three key functional indicators—SIF_{rel}, ET, and VOD_{ratio}—followed by an attribution analysis using the SHAP framework. Prior to model training, feature selection was performed using Mutual Information (MI) to reduce redundancy and enhance predictive power; only variables with MI values greater than 0.1 were retained. The dataset was then split into a combined training–validation set (70%) and a test set (30%). Model hyperparameters were optimized through Randomized Search Cross-Validation with a 5-fold scheme, ensuring robust generalization and minimizing overfitting. Prediction accuracy was evaluated using Mean Squared Error (MSE) and Root Mean Squared Error (RMSE), providing complementary measures of model fit and error magnitude.

Once the Random Forest models were trained, the SHAP method was applied to quantify the marginal contributions of individual predictor variables to variations in each physiological indicator. This analysis was conducted from both a global and a local perspective. At the global level, variable importance was determined by averaging the absolute SHAP values across all observations, thereby identifying the dominant drivers of vegetation physiological responses over the entire study region and period. These dominant drivers typically included hydrometeorological variables—such as soil moisture and VPD—as well as vegetation activity proxies like the physiological components of SIF.

Beyond assessing individual variable importance, SHAP's interaction analysis was used to explore synergistic effects between predictors. For example, the joint influence of VPD and soil moisture on vegetation physiology was examined to reveal how atmospheric water demand and soil water availability together regulate drought responses. Similarly, interactions between temperature and moisture under drought stress were quantified to better understand compound environmental controls.

The analytical workflow therefore links the predictive capability of Random Forest with the interpretability of SHAP, enabling a mechanistic understanding of how climatic and ecological drivers jointly shape vegetation physiological anomalies. By explicitly ranking predictor contributions and disentangling interaction effects, this approach not only quantifies the relative influence of each factor but also illuminates the underlying processes governing ecosystem functional dynamics during drought. To illustrate this formally, the SHAP value ϕ_i for a given feature i is defined as:

$$\varphi_m(v) = \sum_{S \subseteq N \setminus \{m\}} \frac{|S|!(|N| - |S| - 1)!}{|N|!} (v(S \cup \{m\}) - v(S)) \quad (2)$$

where $\phi_m(v)$ represents the contribution of covariate m, N denotes the set of all covariates, S is a subset of N, and $v(S)$ represents the value of that subset.

3. Results and Discussions

3.1. Temporal Dynamics of Vegetation Structural and Physiological Responses Under Arid and Humid Climate Regions

As shown in Figure 3, vegetation in arid climate regions exhibits pronounced temporal variability in both structural and physiological responses to drought. Both LAI and NIRv begin a general downward trend approximately two months before the drought peak. LAI then reaches its minimum more than one month prior to the peak and continues to fluctuate, thereby exhibiting a trough at the drought peak, whereas NIRv attains its minimum approximately four days prior to the drought peak. This temporal divergence suggests that water stress affects canopy structure earlier than canopy photosynthetic activity, likely reflecting constrained leaf expansion and progressive canopy thinning. Concurrently, SIF and SIF_{rel} exhibit continuous fluctuations before reaching their lowest value approximately four days prior to the drought peak, followed by a gradual recovery. The synchronous decline in SIF and LAI suggests that drought stress impacts not only the physical canopy structure but also exacerbates physiological dysfunction by suppressing photosynthetic efficiency.

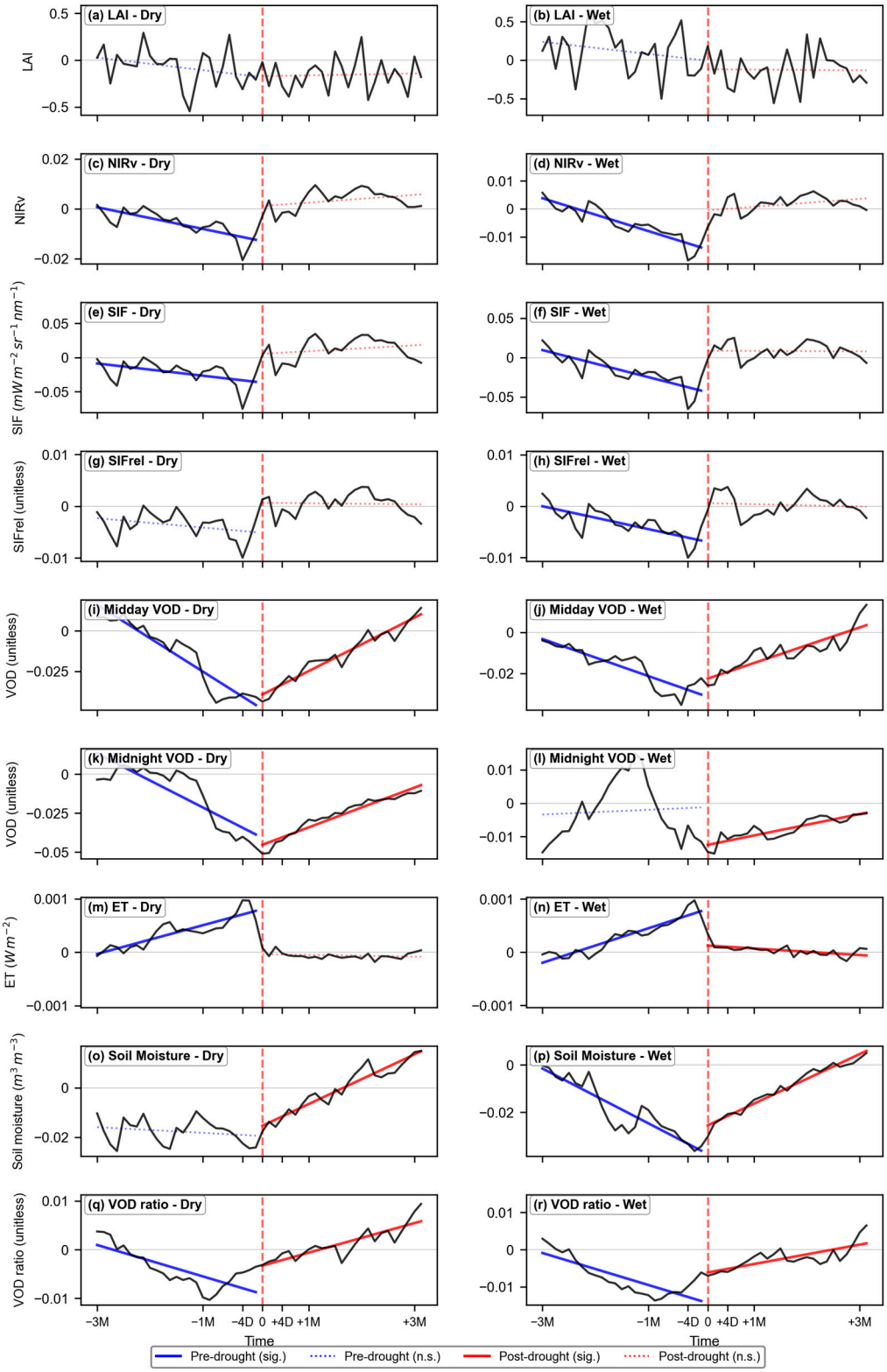


Figure 3. Vegetation index anomaly trajectories under extreme drought conditions across drought-prone (**a**,**c**,**e**,**g**,**i**,**k**,**m**,**o**,**q**) climate zones and (**b**,**d**,**f**,**h**,**j**,**l**,**n**,**p**,**r**) humid regions. (**a**) LAI-Dry; (**b**) LAI-Wet; (**c**) NIRv-Dry; (**d**) NIRv-Wet; (**e**) instantaneous solar-induced chlorophyll fluorescence under clear-sky conditions (SIF_{inst}) in drought prone; (**f**) SIF_{inst} in humid prone; (**g**) SIF_{rel}-Dry; (**h**) SIF_{rel}-Wet; (**i**) Midday VOD-Dry; (**j**) Midday VOD-Wet; (**k**) Midnight VOD-Dry; (**l**) Midnight VOD-Wet; (**m**) ET-Dry; (**n**) ET-Wet; (**o**) Soil Moisture-Dry; (**p**) Soil Moisture-Wet; (**q**) VOD_{ratio}-Dry; (**r**) VOD_{ratio}-Wet;

All variables are presented as anomalies to illustrate the dynamic vegetation responses under drought conditions. Blue and red lines represent the fitted trends for the pre-drought and post-drought periods, respectively. Trend significance is assessed using the Mann–Kendall (MK) test: solid lines indicate statistically significant trends ($p < 0.05$), whereas dashed lines denote non-significant trends. The vertical red dashed line marks the timing of the drought peak.

The VOD, measured both at midday and midnight, shows a consistent pattern of decline in the three months preceding the drought peak, followed by progressive recovery afterward. Notably, the reduction in midnight VOD is more pronounced than at midday, implying a stronger nighttime constraint on vegetation water content under drought stress—potentially due to impaired nocturnal rehydration. Under non-stress conditions, nighttime recovery of vegetation water content is facilitated by reduced transpiration and continued root water uptake, allowing for partial or complete rehydration of plant tissues. However, during drought, this nocturnal rehydration can be strongly constrained by depleted soil moisture and increased hydraulic resistance within the soil–plant continuum. Given that large parts of the study region are dominated by savannas, grasslands, and seasonally dry tropical forests—where isohydric strategies and conservative water-use traits are common—impaired nocturnal rehydration may represent a widespread physiological constraint under extreme drought. The observed midnight VOD sensitivity therefore provides additional insight into ecosystem-level hydraulic regulation that is not captured by daytime signals alone. ET displays an initial increase during the early drought phase (−3M to −1M) and remains elevated through the drought peak, reflecting a shift in the water balance where reduced soil moisture increasingly limits vegetation transpiration, thereby aggravating physiological stress.

In contrast, humid climate regions exhibit a mixed response during comparable drought periods. In humid climate regions, the temporal variations in LAI and NIRv are similar to those observed in arid climate regions. This similarity may be attributed to vegetation acclimation and regulatory processes that moderate canopy structural and functional responses under differing background moisture conditions. The VOD_{ratio} exhibits a declining trend from approximately three months to one month prior to the drought peak, followed by an increasing trend thereafter. This behavior indicates a short-term intensification of diurnal asymmetry in vegetation water status immediately before the drought peak, followed by a stabilization as vegetation adjusts to sustained water stress. Soil moisture shows an overall decreasing trend during the three months preceding the drought peak, reaches its minimum near the drought peak, and then exhibits a general increasing trend during the three months following the peak. This pattern suggests that soil moisture depletion accumulates throughout drought development, attains its maximum severity near the drought peak, and subsequently recovers as drought conditions alleviate. Due to stronger drought adaptability, vegetation in arid regions recovers more rapidly and returns to pre-drought conditions. In contrast, vegetation in humid regions relies more heavily on favorable climatic conditions, resulting in longer recovery times and, in some cases, incomplete recovery to pre-drought levels. This contrast indicates lower drought tolerance and greater drought-induced damage in humid-region vegetation.

Overall, vegetation in arid and humid regions exhibits both shared and contrasting structural and physiological responses to drought, depending on the indicator considered. While water availability plays an important role in shaping ecosystem resilience along the climatic moisture gradient, the observed patterns suggest that vegetation responses are modulated by a combination of background hydroclimatic conditions and adaptive regulatory processes. These findings provide empirical support for mechanistic interpretations of vegetation responses across climatic moisture gradients.

3.2. Spatiotemporal Response Characteristics of Vegetation Physiology to Drought

During drought episodes, ecosystem functional performance and physiological processes exhibit pronounced deviations, as reflected by anomalies in SIF_{rel} (dimensionless), ET (W m^{-2}), and VOD_{ratio} (dimensionless) (Figure 4a–c). Overall, functional anomaly patterns display marked temporal and spatial variability, whereas the physiological anomaly signals—obtained after removing LAI-related structural effects (Figure 4d–f)—isolate the intrinsic physiological adjustments of vegetation under drought stress.

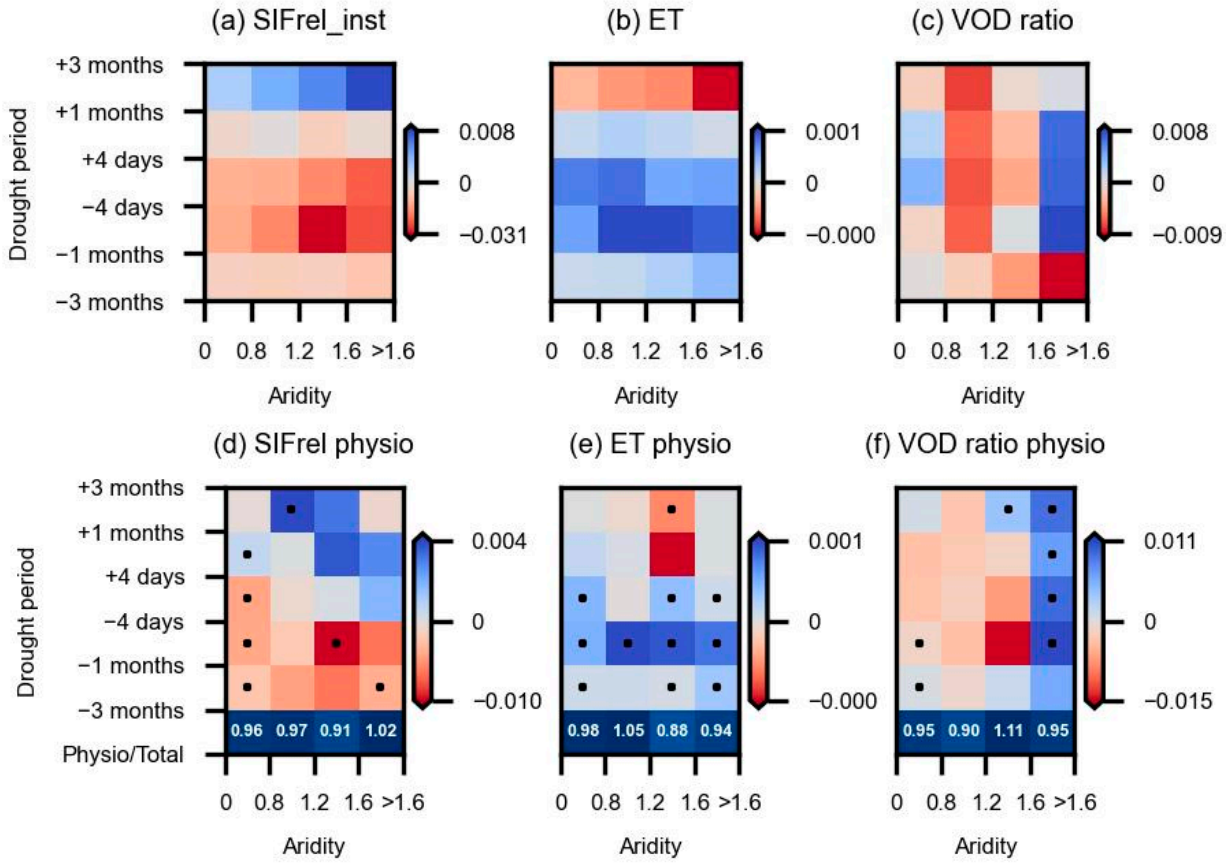


Figure 4. Functional and physiological responses of vegetation to drought: Ecosystem functionality during droughts is reflected by (**a**) SIF_{rel}, (**b**) ET, and (**c**) VOD_{ratio}, while physiological components are derived as (**d**) SIF_{rel}, (**e**) ET, and (**f**) VOD_{ratio} after removing functional anomalies associated with LAI through residual modeling. Each subplot shows the median distribution across specific time windows and aridity grids. Black dots within grids indicate that over 60% of pixels exhibited significant physiological anomalies compared to 1000 random samples within the same season.

During the critical drought period, defined as the interval from three months before the drought peak to one month after the peak, relative solar-induced chlorophyll fluorescence, SIF, exhibits a pronounced negative deviation from the baseline state (Figure 4a), indicating a strong suppression of vegetation photosynthetic activity under water stress conditions. In contrast, evapotranspiration, ET, shows an overall positive anomaly during this period (Figure 4b), suggesting that vegetation maintains elevated water consumption through enhanced transpiration, particularly during the early to middle stages of drought. This response may reflect short-term adaptive regulation to water stress or continued utilization of residual soil moisture. Moreover, differences in ET anomalies across climate zones are relatively small, indicating a high degree of spatial consistency in vegetation evapotranspiration responses to drought and implying regulation by similar physiological control mechanisms. Meanwhile, during the period from three months before the drought

peak to one month after the peak, VOD_{ratio} in humid climate regions exhibits increasing anomaly magnitudes with increasing drought severity, as indicated by the aridity index, with responses transitioning from negative to positive (Figure 4c). This pattern indicates that vegetation in humid regions is more sensitive to changes in water availability during drought development, and that canopy water status and associated functional traits shift from suppression to compensatory responses, potentially related to enhanced deep-root water uptake or strengthened physiological regulation capacity.

When LAI-related variability is excluded, the derived physiological anomaly signals (Figure 4d–f) reveal the independent effects of drought on core physiological processes. The analysis of vegetation physiological anomalies reveals that these anomalies exhibit relatively small spatial variability across regions (Figure 4d–f), indicating a high degree of consistency in physiological responses to drought stress. This result further confirms that regional differences in overall vegetation drought anomalies under different climatic conditions are primarily driven by structural components, whereas physiological components tend to adopt relatively uniform response strategies.

The ratio of physiological anomalies to total functional anomalies (Physio/Total) remains relatively stable across drought severity classes (Figure 4d–f, lower panels). Median Physio/Total values, annotated beneath each time window, show that physiological processes consistently account for a substantial fraction of functional deviations, approaching unity during the most severe phase (+4 days to +1 month). This convergence implies that physiological impairment is the dominant driver of functional decline under extreme drought. Black dots in Figure 4 denote time windows where physiological anomalies differ significantly ($p < 0.05$) from random samples drawn from non-drought years in the same season; notably, over 60% of grid cells exhibit such significant differences (95% confidence interval).

3.3. Spatial Distribution and Response Characteristics of Physiological Anomalies in Different Vegetation Types

Using multi-sensor remote sensing data, this study characterizes the spatial heterogeneity of vegetation physiological anomalies in photosynthesis, evapotranspiration, and water regulation during drought conditions. Spatial patterns of SIF_{rel} and ET anomalies (Figure 5a,b) reveal that the most pronounced physiological deviations are concentrated in the central and southern sectors of the study area, exhibiting clear geographic clustering. VOD_{ratio} anomalies (Figure 5c) are more spatially dispersed, indicating a sparser and more heterogeneous spatial response.

To assess the role of different vegetation types in shaping these spatial patterns, we calculated the proportion of each vegetation type within pixels exhibiting significant anomalies (Figure 5d). The results indicate that grasslands and forests dominate the affected areas for all three indicators. Grasslands account for the largest share of SIF_{rel} and ET anomaly zones. These findings suggest that, in terms of spatial extent, grasslands and forests are the ecosystems most impacted by this drought episode.

We further explored drought-response strategies using boxplot analyses by vegetation type (Figure 5). For SIF_{rel} anomalies (Figure 5a), median values for all vegetation types are negative or near zero, indicating that drought stress generally suppresses regional photosynthetic capacity. Shrublands show the lowest median, signifying severe suppression of photosynthetic function in their responses. In contrast, forests exhibit medians closer to zero with narrower distributions, suggesting more stable photosynthetic performance. Grasslands display a broad anomaly distribution with a median slightly below zero, reflecting substantial within-type heterogeneity.

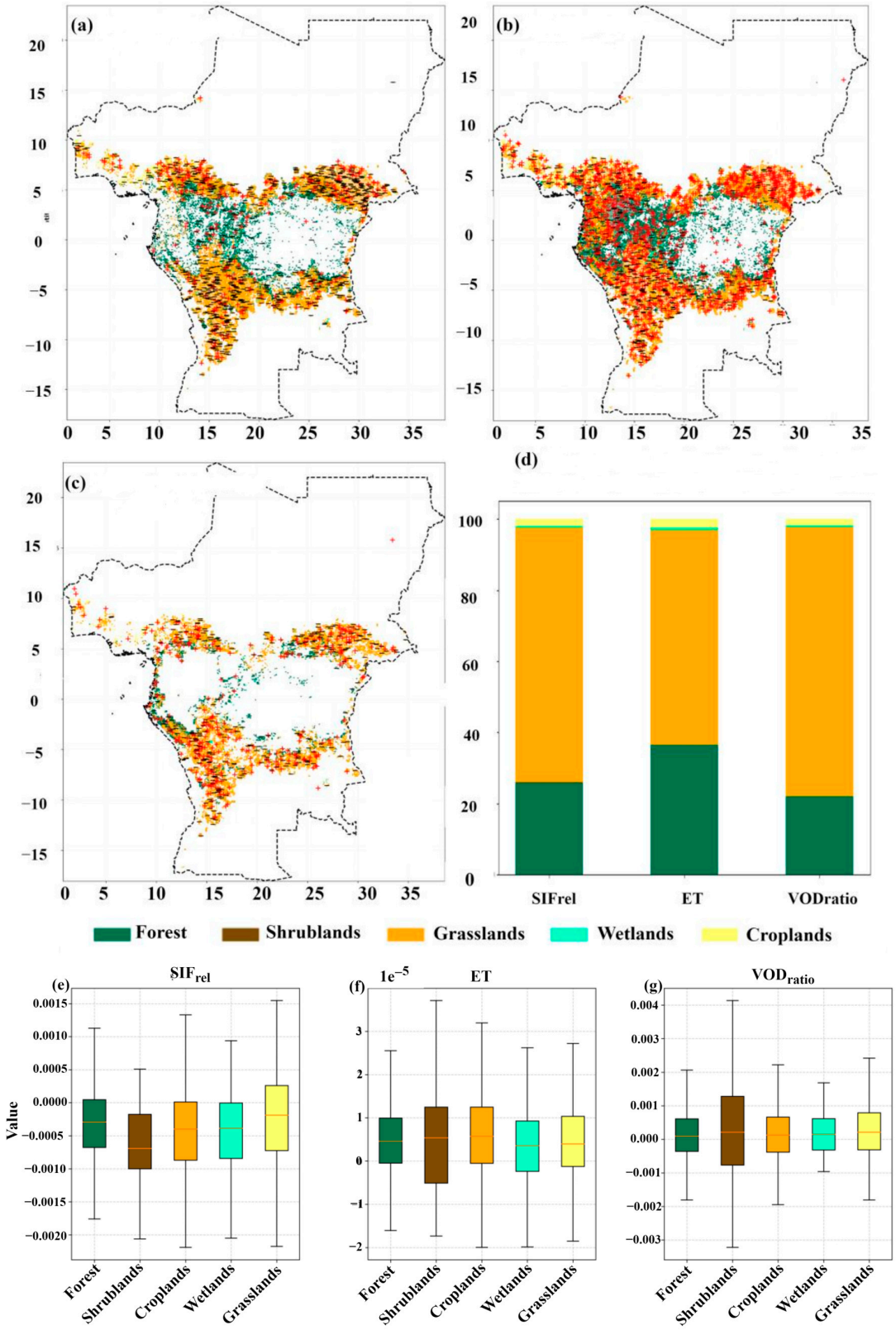


Figure 5. Spatiotemporal Distribution of Drought and Physiological Anomaly Separation Results. (**a**) SIF$_{rel}$ Physiology Anomalies; (**b**) ET Phsysiology Anomalies; (**c**) VOD$_{ratio}$ Phsysiology Anomalies; (**d**) The proportion of each type of vegetation in the three types of phsysiological responses; (**e**) Box plots of the physiological components of SIF$_{rel}$ anomalies; (**f**) Box plots of the physiological components of ET anomalies; (**g**) Box plots of the physiological components of VOD$_{ratio}$ anomalies.

Patterns in ET anomalies (Figure 5b) show distinct responses among vegetation types. The consistently positive median ET anomalies suggest that evapotranspiration tends to be enhanced across vegetation types during the analyzed period, although the magnitude and variability of responses differ among cover classes. Shrublands display relatively large variability in ET anomalies, indicating substantial fluctuations in evapotranspiration. This behavior likely reflects the high sensitivity of shrub-dominated ecosystems to changing atmospheric demand and soil moisture conditions, where flexible stomatal regulation and shallow rooting systems can lead to rapid changes in evapotranspiration under transient moisture availability. In contrast, forests, wetlands, and croplands maintain median ET values near zero with limited variability, potentially due to deep rooting in forests, sustained hydrological inputs in wetlands, or irrigation management in croplands.

VOD_{ratio} anomalies (Figure 5g) reveal particularly distinct water-regulation strategies among vegetation types. A positive VOD_{ratio} anomaly generally signals increased reliance on stored water to sustain physiological activity, thereby reflecting heightened water stress. Shrublands show substantially positive medians, far exceeding other vegetation types, indicating acute pressure on their water-regulation mechanisms. In contrast, forests, wetlands, and grasslands maintain medians near zero with small interquartile ranges, suggesting resilient water regulation that buffers against drought impacts without excessive depletion of internal water reserves.

3.4. The Physiological and Structural Response Ratios of Vegetation Under Drought Conditions: Temporal Variations and Phased Characteristics

To comprehensively characterize the spatiotemporal dynamics of vegetation responses to drought across different climatic regimes, we examined the temporal variation in the contribution ratios of proportions of physiological and structural components within three key vegetation indicators—SIF_{rel}, ET, and VOD_{ratio}—throughout drought events (Figure 6a–f). Additionally, a heatmap visualization (Figure 6g–i) summarizes these patterns across three drought phases: pre-drought, peak-drought, and post-drought.

The contribution ratio quantifies the relative importance of each response mechanism and is calculated as the proportion of the absolute magnitude of each component to their combined total. This metric ensures that the two ratios sum to 100%, thereby quantifying the relative contributions of rapid physiological adjustments—such as stomatal closure and photosynthetic regulation—and slower structural modifications, including leaf area reduction and biomass loss, within the total vegetation response. In the three months before and after the drought peak (Figure 6a,c,e), vegetation responses were predominantly physiological, particularly in humid regions where the contribution of physiological processes far exceeded that of structural changes. At the drought peak, the physiological share increased further and displayed greater temporal variability, suggesting intensified short-term regulation—such as stomatal control of transpiration and adjustments in photosynthetic efficiency—to mitigate drought-induced stress.

The heatmaps in Figure 6g–i corroborate this pattern: the first and third rows of each heatmap display the "Physio/Total" ratio, which ranges from 0 to 1, with values approaching 1 indicating physiological dominance. The results show that such physiological dominance was consistent across all indicators during the three months preceding the drought peak, with similar tendencies observed in both arid and humid zones. This highlights that prior to the onset of severe stress, vegetation predominantly employs rapid physiological adjustments as its primary adaptive mechanism.

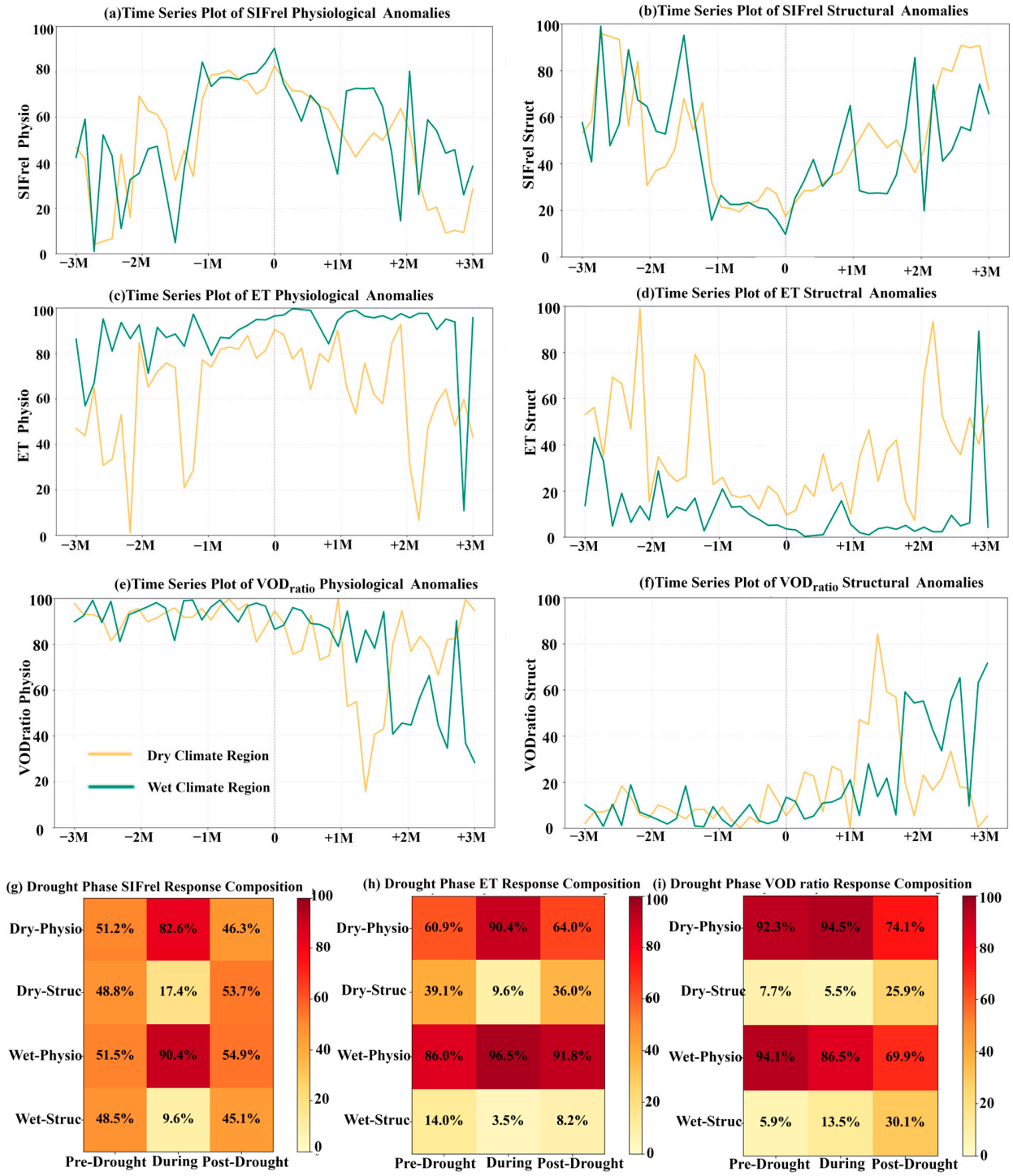


Figure 6. Panels (**a**–**f**) present the time series of correlation ratios (%) for three variables—SIF$_{rel}$, ET, and VOD$_{ratio}$—separated into physiological (left) and structural (right) anomalies for dry (red line) and wet (blue line) regions. The *x*-axis represents time centered around drought events (in months), with '0" marking the drought peak. Panels (**g**–**i**) depict the drought phase-wise composition of dominant responses (physiological vs. structural) for each variable in both dry and wet regions. Each heatmap shows the percentage contribution of physiological and structural responses during pre-drought, drought, and post-drought phases.

However, a distinct shift is observed in VOD_{ratio} after the drought peak. Both the proportional time-series (Figure 6e,f) and heatmap (Figure 6i) reveal a marked increase in structural responses, indicating substantial canopy and biomass adjustments under prolonged or extreme water deficits. Importantly, the delayed enhancement of structural responses following drought indicates a temporally lagged adjustment of canopy structure relative to rapid physiological stress responses. Such structural lags may represent a meaningful indicator of longer-term ecosystem change, as persistent or recurrent post-drought structural degradation can result in sustained reductions in vegetation cover and biomass, thereby increasing the likelihood of vegetation browning. However, whether these short-term, event-scale structural responses ultimately translate into enduring ecosystem shifts is likely contingent upon drought frequency, the duration and effectiveness of post-drought recovery, and the intrinsic resilience of vegetation communities.

3.5. Attribution Analysis of Physiological Responses

3.5.1. Feature Selection and Model Evaluation

To explore the interpretability of the model, we used the SHAP method to calculate the contribution proportions of each feature to the changes in the target variables, as summarized in Figure 7. These values represent the normalized contribution of environmental predictors (precipitation, temperature, soil moisture, VPD, and radiation) to the total model predictions. Specifically, for each target variable at each pixel and time step, we calculated the absolute SHAP values for all environmental factors, summed them, and divided by the sum of absolute SHAP values from all predictors (including both environmental and vegetation structural factors). The reported proportions are spatially averaged across all valid pixels (vegetation cover > 0.05 and irrigation < 10%) within the study area. Before and after the drought, the contribution proportions of environmental factors to the target variables SIF_{rel}, ET, and VOD_{ratio} were as follows: 0.7680, 0.6027, and 0.5394 (during drought development) and 0.6356, 0.6030, and 0.8678 (during drought recovery). These results indicate that the contribution of environmental factors to vegetation physiological indicators varies significantly across different stages of drought, especially during the drought recovery stage, where the environmental variables have a particularly prominent impact on vegetation water and photosynthesis.

3.5.2. SHAP Attribution Analysis and the Influence of Environmental Factor

The SHAP analysis identifies precipitation as the dominant driver of SIF_{rel} variability, primarily through its control over soil moisture and, consequently, plant water availability. Reduced precipitation limits soil water supply, constraining stomatal conductance and photosynthetic carbon assimilation. Temperature and soil moisture rank next in importance: elevated temperatures increase atmospheric evaporative demand, while reduced soil moisture directly limits root water uptake, intensifying drought stress. Although VPD and radiation exert smaller overall effects, their roles remain ecologically significant. Elevated VPD induces stomatal closure, restricting CO_2 uptake, whereas excessive radiation can exacerbate leaf heating, further suppressing photosynthesis. Collectively, these factors constrain SIF_{rel}, making it a sensitive early warning signal of drought-induced stress. Soil moisture availability emerges as the most critical factor for SIF_{rel} recovery, with recovery duration also determining restoration efficiency. Compared with the drought development phase, the relative influence of temperature and VPD declines during recovery, suggesting that intrinsic physiological repair mechanisms dominate once water availability is restored—although extreme thermal conditions can still delay full recovery.

For ET, temperature exerts the strongest influence during the drought phase. Prolonged drought, coupled with reduced precipitation, depletes soil moisture, prompting water-conservation strategies (e.g., stomatal closure) that ultimately reduce ET despite high evaporative demand. VPD exacerbates this effect by further increasing atmospheric moisture demand. During recovery, soil moisture becomes the primary driver of ET restoration, while VPD and recovery duration also play significant roles. Optimal temperatures facilitate this re-coupling between water supply and atmospheric demand, enabling faster ET recovery.

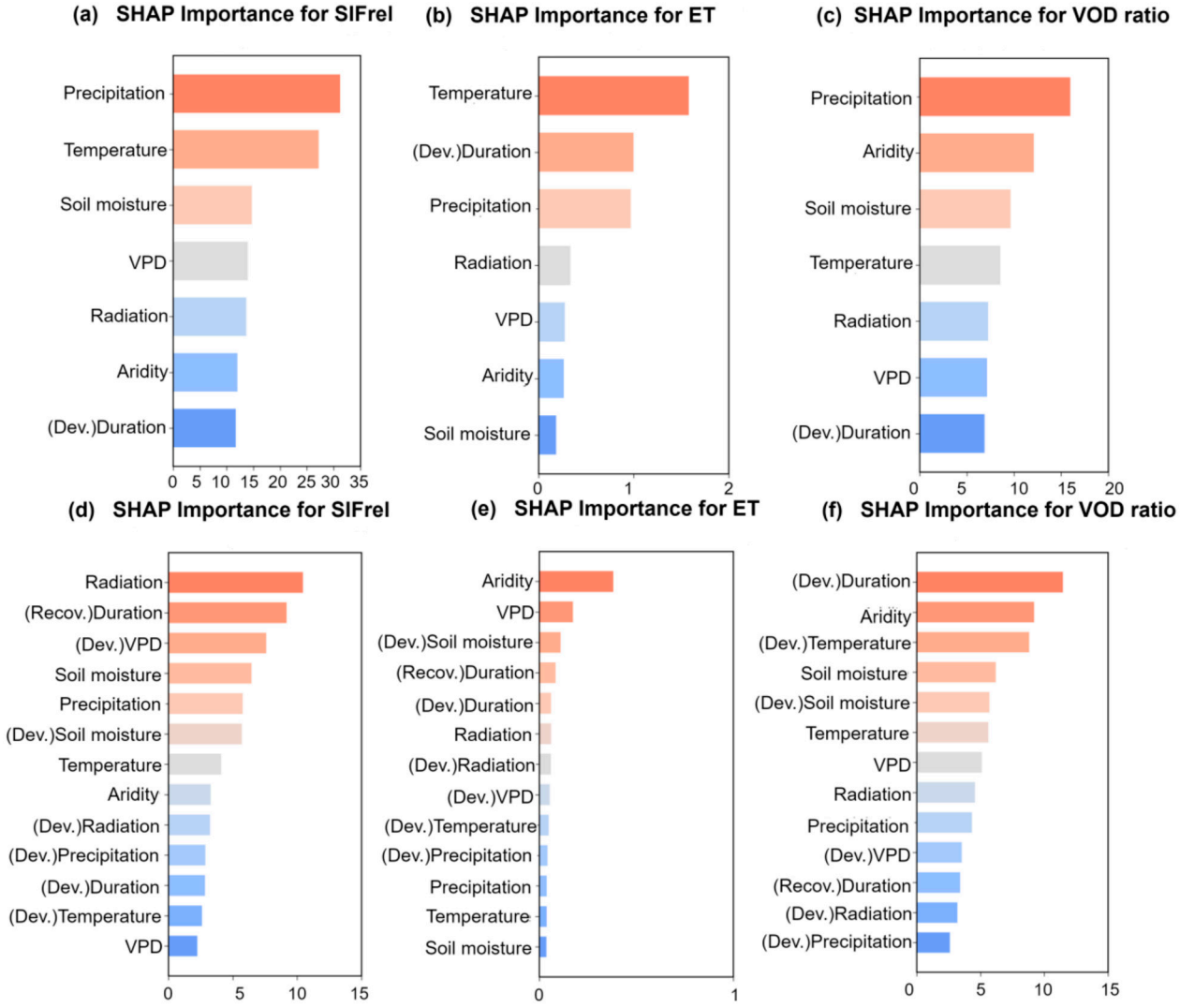


Figure 7. Analysis of Drivers of Vegetation Physiological Anomalies Under Drought Conditions: The drivers include mean climate and vegetation characteristics, as well as hydrometeorological anomalies related to drought and drought duration. Panels (**a**–**c**) show the relative importance of these factors in explaining the spatial variability of physiological anomalies in the ratios of SIF_{rel}, ET, and VOD_{ratio} during the drought development phase. Panels (**d**–**f**) display the corresponding analysis for the drought recovery phase, illustrating the duration of drought and hydrometeorological anomalies associated with the development (Dev.) and recovery (Recov.) phases. The relative importance of all physiological variables is expressed in the same units to allow for direct comparison.

In the case of VOD_{ratio}, precipitation is the most influential factor during drought onset and progression, with reduced rainfall directly lowering vegetation water content. Drought intensity and soil moisture exert additional strong effects, while temperature influences VOD_{ratio} indirectly via increased evaporative demand. During recovery, recovery duration

is the most critical factor, with longer periods allowing for gradual rehydration and canopy regrowth. During the early recovery stage spanning days to weeks, increases in VOD_{ratio} are primarily driven by rapid physiological processes such as plant tissue rehydration and cell expansion. As recovery progresses, hydraulic structural recovery processes including the restoration of leaf water transport systems and the alleviation of xylem embolism gradually become dominant. Over longer recovery periods, structural recovery processes such as new leaf flushing and canopy rebuilding further promote VOD_{ratio} toward its baseline level. Therefore, the increasing importance of recovery duration reflects a multi-stage vegetation recovery trajectory that transitions from rapid physiological regulation to medium- and long-term structural rebuilding. The changing sensitivity of VOD_{ratio} to recovery duration highlights its role as an integrated indicator that responds to both plant water status and biomass dynamics and is able to capture recovery processes across multiple scales from the cellular level to the canopy scale.

When jointly analyzing the driving factors during both the drought development and recovery stages, we found that precipitation, temperature, and soil moisture continue to play important roles for SIF_{rel}. For ET, the importance of VPD, aridity, and soil moisture increases. Notably, for SIFrel, ET, and VOD_{ratio}, the duration of the recovery period plays an important role during the drought recovery stage, particularly for SIFrel and VOD_{ratio}. Moreover, compared with the drought development stage, the importance of recovery duration in shaping the physiological responses of SIF_{rel} and VOD_{ratio} increases significantly during the recovery period.

Across all indicators, vegetation often experiences multiple concurrent stressors, and their combined impacts are frequently synergistic rather than additive. For example, compound drought–heat events cause more severe physiological impairment and prolong recovery compared to drought alone, with high VPD amplifying water stress and further suppressing photosynthesis. Such interactions underline the vulnerability of plant physiological systems to multi-stressor environments. Understanding these dynamics is essential for improving predictions of ecosystem drought responses and for designing effective water–land management and climate adaptation strategies.

While the present study reveals distinct structural and physiological drought responses across climatic gradients using multi-source remote sensing data, the relatively limited temporal resolution constrains our ability to fully capture rapid vegetation dynamics and short-term adaptive processes. Therefore, future research should prioritize higher temporal and spatial resolution observations, together with multi-dimensional and multi-process analyses, to further elucidate plant adaptation mechanisms across different ecosystems under drought stress.

4. Conclusions

This study disentangled African vegetation's physiological and structural responses to drought using a random forest-based anomaly decomposition framework. The results indicate that physiological anomalies accounted for a large proportion of the observed functional anomalies during peak drought. This finding suggests that within the context of our analysis, rapid physiological regulation may play a more prominent role than structural adjustments in shaping short-term vegetation responses to drought, complementing previous studies that have emphasized longer-term canopy structural changes [35].

By integrating vegetation indicators with hydrometeorological drivers, our multi-model and SHAP-based attribution analysis identified precipitation as the dominant control on photosynthesis and vegetation water status during drought development, with soil moisture and temperature exerting secondary but reinforcing influences. For SIF_{rel}, ET, and VOD_{ratio}, the duration of the recovery period emerges as an important driver during drought recovery, with particularly strong effects for SIF_rel and VOD_{ratio}. Furthermore, relative to the drought development stage, the influence of recovery duration on the physiological responses of SIF_{rel} and VOD_{ratio} increases markedly during the recovery phase.

Spatially, drought impacts were most pronounced in semi-arid and transitional zones, where increased water competition and atmospheric demand strongly suppressed photosynthesis and water use. Humid regions showed fewer anomalies, reflecting higher drought resistance. Across vegetation types, shrublands exhibited the lowest resilience, with severe and unstable variability in photosynthesis, evapotranspiration, and water regulation. Grasslands and forests contributed most to the spatial extent of anomalies but through distinct strategies—forests maintained stability via deep rooting, while grasslands displayed high variability due to their shallow-rooted, moisture-sensitive nature.

Methodologically, combining machine learning with explainable AI overcame long-standing barriers to separating physiological from structural signals, delivering unprecedented functional-level resolution (0.05°/4-day) compared to conventional drought indices like VegDRI. Theoretically, our results refine drought-response theory by establishing the phased dominance of physiological processes within ± 3 months of drought peaks. Practically, this approach enables more timely and targeted monitoring for ecosystem and water-resource management.

Overall, water availability emerged as the core driver of vegetation drought responses, with distinct climatic and ecological controls during development versus recovery stages. These findings provide new theoretical insights, robust observational evidence, and actionable guidance for sustainable water and land management in African ecosystems under climate change. Future work should integrate this framework with the Coupled Model Intercomparison Project Phase 6 (CMIP6) projections to assess how physiological dominance may shift under elevated CO_2 and more frequent compound drought–heat extremes.

Author Contributions: Conceptualization, X.Z. and Y.Z.; methodology, X.Z. and Y.Z.; software, Y.Z.; formal analysis, Y.Z.; investigation, Y.Z.; resources, X.Z. and Y.Z.; data curation, Y.Z.; writing—original draft preparation, Y.Z.; writing—review and editing, X.Z. and Y.Z.; visualization, Y.Z.; supervision, X.Z. and Y.Z.; project administration, X.Z. and Y.Z. All authors have read and agreed to the published version of the manuscript.

Funding: This work was supported by Natural Science Foundation of China (Grant No 42461144214; 42471349), Guangdong Basic and Applied Research Foundation (Grant No 2024A1515030078), Shenzhen Science and Technology Program (Grant No JCYJ20240813114013017), Natural Science Foundation of Wuhan (Grant No 2024040801020279), and Guided Project of Hubei Provincial Department of Education (Grant No B2023246).

Data Availability Statement: Data will be made available on request.

Acknowledgments: The authors thank the anonymous reviewers for their constructive comments and suggestions. We also acknowledge the providers of the remote sensing and climate datasets used in this study.

Conflicts of Interest: The authors declare no conflicts of interest.

Appendix A

Table A1. Comparison of vegetation drought response studies.

Source	Study Area	Time Span	Spatial Resolution	Temporal Resolution	Remote Sensing Data	Method	Contribution	Key Findings	Comments
(Jesslyn et al., 2008) [36]	U.S. Great Plains	1989–2005	1 km	14 days	Standardized Precipitation Index, Palmer Drought Severity Index, Percent of Average Seasonal Greenness, etc.	Supervised classification and regression tree (CART/Cubist)	Comprehensive monitoring index for vegetation drought stress	Provides 1 km drought condition maps	A composite drought assessment; no disentanglement of structural vs. physiological impacts
(Vicente-Serrano et al., 2013) [37]	Global terrestrial biomes	Not specified	Multi-scale	Multi-scale	Vegetation indices, tree rings, ANPP, SPEI	Correlation analysis	Assessing biome-specific drought responses; emphasizing temporal scales	Arid/humid biomes respond rapidly to short-term drought; semi-arid/sub-humid biomes respond to long-term drought	Macro-scale global focus; lacks regional mechanistic details and functional decoupling
(Sevanto et al., 2014) [38]	Drylands, eucalypt, tropical forests	Long-term	Global/conceptual	no specific resolution	NDVI, kNDVI, NIRv, LAI, VOD, SIF; meteorological, soil data	Mechanistic and conceptual framework	Drought-induced tree mortality mechanisms; process-based models	Tree mortality from hydraulic/carbon/biotic stress; process models explain best	Only correlations but lacks fine-scale decoupling of physiological vs. structural responses
Prentice et al. (2017) [39]	Global continental scale (e.g., SW N. America, Amazon)	140 years	1°	Monthly, annual	P-ET, ET, EF, soil moisture, LAI, net radiation (R_n), VPD	CMIP5 ESMs; idealized single-forcing experiments, linear decomposition	Relative roles of CO_2-induced physiological effects vs. atmospheric changes on hydrology	CO_2 effects dominate ET/EF, impacting runoff beyond climate, coupling carbon-water cycles	Macro-scale global focus; lacks regional mechanistic details and functional decoupling
(Jiao et al., 2021) [40]	Northern Hemisphere temperate zones	1982–2015	0.5°	Monthly	SIF, GPP, NDVI, VOD, EVI, meteorological data	Correlation, response time, and attribution analysis	Quantifying vegetation response to water variability; analyzing drivers	Widespread increase in water limitation; shorter vegetation response time to moisture stress. Precipitation and solar radiation are key drivers	Only correlations analysis but lacks fine-scale decoupling of physiological vs. structural responses
(Kannenberg et al., 2022) [41]	North America and Europe	2002–2019	Not specified	Annual	Tree-ring width, GPP, LAI	Empirical analysis of resistance/recovery indices	Decoupling carbon uptake (GPP) and tree growth; drought legacy effects	GPP is relatively drought-resistant, while structural growth is more sensitive; decoupling persists as a legacy effect	Focuses on GPP vs. structural growth but may miss high-resolution functional changes (e.g., SIF/VOD)
(Maedeh et al., 2023) [42]	Ecosystem scale	Not specified	Ecosystem scale	Multi-scale	VOD, SIF	Complementarity assessment; plant-strategy interpretation	Evaluating VOD and SIF as complementary signals; revealing drought strategies	VOD and SIF reveal divergent early responses: SIF-sensitive in isohydric plants, VOD-sensitive in anisohydric plants	Predicts seasonal agricultural drought but lacks functional-level dissection of vegetation response mechanisms
(Xu et al., 2024) [43]	Global (agricultural sector)	2000–2020	1.5°	1 day	ECMWF S2S model meteorological data	Stacked ML ensemble (CBR, ETR, XGB, LGBM, RF)	Machine learning for robust seasonal drought prediction	Strong correlation ($R^2 > 0.8$) in seasonal drought prediction; standardized agricultural drought protocol	Predicts seasonal agricultural drought but lacks functional-level dissection of vegetation response mechanisms
This paper	Central and West Africa	2012–2020	0.05°	4 days	ET, SIF_{rel}, VOD_{ratio}, LAI	Multi-model framework; random forest for signal decomposition and driver identification	Decoupling structural and physiological responses; phased water regulation; driver identification	Physiological responses dominate three months before and after peak growing period; drought responses show phased characteristics; vegetation responses influenced by precipitation, temperature, etc.	Decouples physiological and structural responses, emphasizes physiological dominance, and uses SHAP for interpretable attribution, surpassing traditional methods

References

1. Vicente-Serrano, S.M.; Quiring, S.M.; Peña-Gallardo, M.; Yuan, S.; Domínguez-Castro, F. A review of environmental droughts: Increased risk under global warming? *Earth-Sci. Rev.* **2020**, *201*, 102953. [CrossRef]
2. Lombe, P.; Carvalho, E.; Rosa-Santos, P. Drought Dynamics in Sub-Saharan Africa: Impacts and Adaptation Strategies. *Sustainability* **2024**, *16*, 9902. [CrossRef]
3. Zhu, Z.; Piao, S.; Myneni, R.B.; Huang, M.; Zeng, Z.; Canadell, J.G.; Ciais, P.; Sitch, S.; Friedlingstein, P.; Arneth, A.; et al. Greening of the Earth and its drivers. *Nat. Clim. Change* **2016**, *6*, 791–795. [CrossRef]
4. Zhou, G.-Y.; Zhou, L.-Y.; Shao, J.-J.; Zhou, X.-H. Effects of extreme drought on terrestrial ecosystems: Review and prospects. *Chin. J. Plant Ecol.* **2020**, *44*, 515–525. [CrossRef]
5. Li, W.; Pacheco-Labrador, J.; Migliavacca, M.; Miralles, D.; Hoek van Dijke, A.; Reichstein, M.; Forkel, M.; Zhang, W.; Frankenberg, C.; Panwar, A.; et al. Widespread and complex drought effects on vegetation physiology inferred from space. *Nat. Commun.* **2023**, *14*, 4640. [CrossRef] [PubMed]
6. Hao, H.; Hao, X.; Xu, J.; Chen, Y.; Zhao, H.; Li, Z.; Kayumba, P.M. Recent Response of Vegetation Water Use Efficiency to Climate Change in Central Asia. *Remote Sens.* **2022**, *14*, 5999. [CrossRef]
7. Liu, Z.; Chen, L.; Smith, N.G.; Yuan, W.; Chen, X.; Zhou, G.; Alam, S.A.; Lin, K.; Zhao, T.; Zhou, P.; et al. Global divergent responses of primary productivity to water, energy, and CO_2. *Environ. Res. Lett.* **2019**, *14*, 124044. [CrossRef]
8. Frank, D.; Reichstein, M.; Bahn, M.; Thonicke, K.; Frank, D.; Mahecha, M.D.; Smith, P.; van der Velde, M.; Vicca, S.; Babst, F.; et al. Effects of climate extremes on the terrestrial carbon cycle: Concepts, processes and potential future impacts. *Glob. Change Biol.* **2015**, *21*, 2861–2880. [CrossRef]
9. Liu, Y.; Konings, A.G.; Kennedy, D.; Gentine, P. Global Coordination in Plant Physiological and Rooting Strategies in Response to Water Stress. *Global Biogeochem. Cycles* **2021**, *35*, 6758. [CrossRef]
10. Ding, Y.; Nie, Y.; Chen, H.; Wang, K.; Querejeta, J.I. Water uptake depth is coordinated with leaf water potential, water-use efficiency and drought vulnerability in karst vegetation. *New Phytol.* **2021**, *229*, 1339–1353. [CrossRef]
11. Sobejano-Paz, V.; Mikkelsen, T.N.; Baum, A.; Mo, X.; Liu, S.; Köppl, C.J.; Johnson, M.S.; Gulyas, L.; García, M. Hyperspectral and Thermal Sensing of Stomatal Conductance, Transpiration, and Photosynthesis for Soybean and Maize under Drought. *Remote Sens.* **2020**, *12*, 3182. [CrossRef]
12. Damm, A.; Paul-Limoges, E.; Haghighi, E.; Simmer, C.; Morsdorf, F.; Schneider, F.D.; van der Tol, C.; Migliavacca, M.; Rascher, U. Remote sensing of plant-water relations: An overview and future perspectives. *J. Plant Physiol.* **2018**, *227*, 3–19. [CrossRef] [PubMed]
13. Xu, H.J.; Wang, X.P.; Zhao, C.Y.; Yang, X.M. Assessing the response of vegetation photosynthesis to meteorological drought across northern China. *Land Degrad. Dev.* **2020**, *32*, 20–34. [CrossRef]
14. Hoek van Dijke, A.J.; Orth, R.; Teuling, A.J.; Herold, M.; Schlerf, M.; Migliavacca, M.; Machwitz, M.; van Hateren, T.C.; Yu, X.; Mallick, K. Comparing forest and grassland drought responses inferred from eddy covariance and Earth observation. *Agric. For. Meteorol.* **2023**, *341*, 109635. [CrossRef]
15. Gu, H.; Yin, G.; Yang, Y.; Verger, A.; Descals, A.; Filella, I.; Zeng, Y.; Hao, D.; Xie, Q.; Li, X.; et al. Satellite-Detected Contrasting Responses of Canopy Structure and Leaf Physiology to Drought. *IEEE J. Sel. Top. Appl. Earth Obs. Remote Sens.* **2023**, *16*, 2427–2436. [CrossRef]
16. Schmidt, L.; Forkel, M.; Zotta, R.-M.; Scherrer, S.; Dorigo, W.A.; Kuhn-Régnier, A.; van der Schalie, R.; Yebra, M. Assessing the sensitivity of multi-frequency passive microwave vegetation optical depth to vegetation properties. *Biogeosciences* **2023**, *20*, 1027–1046. [CrossRef]
17. Yao, Y.; Humphrey, V.; Konings, A.G.; Wang, Y.; Yin, Y.; Holtzman, N.; Wood, J.D.; Bar-On, Y.; Frankenberg, C. Investigating Diurnal and Seasonal Cycles of Vegetation Optical Depth Retrieved from GNSS Signals in a Broadleaf Forest. *Geophys. Res. Lett.* **2024**, *51*, 7121. [CrossRef]
18. Momen, M.; Wood, J.D.; Novick, K.A.; Pangle, R.; Pockman, W.T.; McDowell, N.G.; Konings, A.G. Interacting Effects of Leaf Water Potential and Biomass on Vegetation Optical Depth. *J. Geophys. Res. Biogeosci.* **2017**, *122*, 3031–3046. [CrossRef]
19. Nicholson, S.E.; Tucker, C.J.; Ba, M.B. Desertification, Drought, and Surface Vegetation: An Example from the West African Sahel. *Bull. Am. Meteorol. Soc.* **1998**, *79*, 815–830. [CrossRef]
20. Thorncroft, C.D.; Nguyen, H.; Zhang, C.; Peyrillé, P. Annual cycle of the West African monsoon: Regional circulations and associated water vapour transport. *Q. J. R. Meteorol. Soc.* **2011**, *137*, 129–147. [CrossRef]
21. Sultan, B.; Janicot, S. Abrupt Shift of the ITCZ over West Africa and intra-seasonal variability. *Geophys. Res. Lett.* **2000**, *2720*, 3353–3356. [CrossRef]
22. Malhi, Y.; Adu-Bredu, S.; Asare, R.A.; Lewis, S.L.; Mayaux, P. African rainforests: Past, present and future. *Philos. Trans. R. Soc. B* **2013**, *368*, 312. [CrossRef]
23. Verheggen, A.; Mayaux, P.; de Wasseige, C.; Defourny, P. Mapping Congo Basin vegetation types from 300m and 1km multi-sensor time series for carbon stocks and forest areas estimation. *Biogeosciences* **2012**, *9*, 5061–5079. [CrossRef]

24. Hickler, T.; Eklundh, L.; Seaquist, J.W.; Smith, B.; Ardö, J.; Olsson, L.; Sykes, M.T.; Sjöström, M. Precipitation controls Sahel greening trend. *Geophys. Res. Lett.* **2005**, *32*, 24370. [CrossRef]
25. Rishmawi, K.; Prince, S.D.; Xue, Y. Vegetation Responses to Climate Variability in the Northern Arid to Sub-Humid Zones of Sub-Saharan Africa. *Remote. Sens.* **2016**, *8*, 910. [CrossRef]
26. Zhou, L.; Tian, Y.; Myneni, R.B.; Ciais, P.; Saatchi, S.; Liu, Y.Y.; Piao, S.; Chen, H.; Vermote, E.F.; Song, C.; et al. Widespread decline of Congo rainforest greenness in the past decade. *Nature* **2014**, *509*, 86–90. [CrossRef] [PubMed]
27. Xiao, J.; Terrer, C.; Gentine, P.; Tateno, R.; Fan, L.; Ma, M.; Yue, Y.; Yuan, W.; Peňuelas, J.; Shi, W. Temporal and Phenological Modulation of the Impact of Increasing Drought Conditions on Vegetation Growth in a Humid Big River Basin: Insights from Global Comparisons. *Earth's Future* **2025**, *13*, 5720. [CrossRef]
28. Davidson, E.A.; Araújo, A.C.d.; Artaxo, P.; Balch, J.K.; Brown, I.F.; Bustamante, M.M.C.; Coe, M.T.; DeFries, R.S.; Keller, M.; Longo, M.; et al. The Amazon basin in transition. *Nature* **2012**, *481*, 321–328. [CrossRef]
29. Daniela, V.; Giuseppe, L.-M.; Oscar Rosario, B.; Juan Miguel, R.-C.; Salvatore, P.; Simona, C.; Guido, D.U.; Giovanni Battista, C.; Antonio, C.; Alessandro, C.; et al. Comparing the use of ERA5 reanalysis dataset and ground-based agrometeorological data under different climates and topography in Italy. *J. Hydrol. Reg. Stud.* **2022**, *42*, 101182. [CrossRef]
30. Du, J.; Kimball, J.S.; Jones, L.A.; Kim, Y.; Glassy, J.; Watts, J.D. A global satellite environmental data record derived from AMSR-E and AMSR2 microwave Earth observations. *Earth Syst. Sci. Data* **2017**, *9*, 791–808. [CrossRef]
31. Cao, J.; Luo, Y.; Zhang, X.; Fan, L.; Tao, J.; Nam, W.-H.; Sur, C.; He, Y.; Gulakhmadov, A.; Niyogi, D. Assessing the responsiveness of multiple microwave remote sensing vegetation optical depth indices to drought on crops in Midwest US. *Int. J. Appl. Earth Obs. Geoinf.* **2024**, *132*, 104072. [CrossRef]
32. Yifan, D.; Donghong, X.; Zhengan, S.; Xingwu, D.; Xiaoning, L.; Su, Z.; Yong, Y. The influences of mass failure on the erosion and hydraulic processes of gully headcuts based on an in situ scouring experiment in Dry-hot valley of China. *Catena* **2019**, *176*, 14–25. [CrossRef]
33. Altman, N.; Krzywinski, M. Ensemble methods: Bagging and random forests. *Nat. Methods* **2017**, *14*, 933–934. [CrossRef]
34. Oshiro, T.M.; Perez, P.S.; Baranauskas, J.A. How Many Trees in a Random Forest? In *Machine Learning and Data Mining in Pattern Recognition*; Springer: Cham, Switzerland, 2012; pp. 154–168.
35. Yu, X.; Orth, R.; Reichstein, M.; Bahn, M.; Klosterhalfen, A.; Knohl, A.; Koebsch, F.; Migliavacca, M.; Mund, M.; Nelson, J.A.; et al. Contrasting drought legacy effects on gross primary productivity in a mixed versus pure beech forest. *Biogeosciences* **2022**, *19*, 4315–4329. [CrossRef]
36. Brown, J.F.; Wardlow, B.D.; Tadesse, T.; Hayes, M.; Reed, B.C. The Vegetation Drought Response Index (VegDRI): A New Integrated Approach for Monitoring Drought Stress in Vegetation. *GISci. Remote Sens.* **2008**, *45*, 16–46. [CrossRef]
37. Vicente-Serrano, S.M.; Gouveia, C.; Camarero, J.J.; Begueria, S.; Trigo, R.; Lopez-Moreno, J.I.; Azorin-Molina, C.; Pasho, E.; Lorenzo-Lacruz, J.; Revuelto, J.; et al. Response of vegetation to drought time-scales across global land biomes. *Proc. Natl. Acad. Sci. USA* **2013**, *110*, 52–57. [CrossRef] [PubMed]
38. Sevanto, S.; McDowell, N.G.; Dickman, L.T.; Pangle, R.; Pockman, W.T. How do trees die? A test of the hydraulic failure and carbon starvation hypotheses. *Plant Cell Environ.* **2014**, *37*, 153–161. [CrossRef]
39. Prentice, I.C.; Cleator, S.F.; Huang, Y.H.; Harrison, S.P.; Roulstone, I. Reconstructing ice-age palaeoclimates: Quantifying low-CO2 effects on plants. *Glob. Planet. Change* **2017**, *149*, 166–176. [CrossRef]
40. Jiao, W.; Wang, L.; Smith, W.K.; Chang, Q.; Wang, H.; D'Odorico, P. Observed increasing water constraint on vegetation growth over the last three decades. *Nat. Commun.* **2021**, *12*, 3777. [CrossRef] [PubMed]
41. Kannenberg, S.; Cabon, A.; Babst, F.; Belmecheri, S.; Delpierre, N.; Guerrieri, R.; Maxwell, J.; Meinzer, F.; Moore, D.; Pappas, C.; et al. Drought-induced decoupling between carbon uptake and tree growth impacts forest carbon turnover time. *Agric. For. Meteorol.* **2022**, *322*, 108996. [CrossRef]
42. Maedeh, B.; Kakroodi, A.A.; Majid, K.; Ghasem, A. Satellite-based drought monitoring using optimal indices for diverse climates and land types. *Ecol. Inform.* **2023**, *76*, 102143. [CrossRef]
43. Xu, L.; Zhang, X.; Wu, T.; Yu, H.; Du, W.; Zhang, C.; Chen, N. Global Prediction of Flash Drought Using Machine Learning. *Geophys. Res. Lett.* **2024**, *51*, e2024GL111134. [CrossRef]

Disclaimer/Publisher's Note: The statements, opinions and data contained in all publications are solely those of the individual author(s) and contributor(s) and not of MDPI and/or the editor(s). MDPI and/or the editor(s) disclaim responsibility for any injury to people or property resulting from any ideas, methods, instructions or products referred to in the content.